Anomalous thermal transport and strong violation of Wiedemann-Franz law in the critical regime of a charge density wave transition

Erik D. Kountz [1,2,3] Jiecheng Zhang,[1,2,3] Joshua A. W. Straquadine [1,2,4] Anisha G. Singh,[1,2,4] Maja D. Bachmann,[1,2,4]
Ian R. Fisher,[1,2,4] Steven A. Kivelson [1,2,3] and Aharon Kapitulnik[1,2,3,4]

[1]*Stanford Institute for Materials and Energy Sciences, SLAC National Accelerator Laboratory,*
2575 Sand Hill Road, Menlo Park, California 94025, USA
[2]*Geballe Laboratory for Advanced Materials, Stanford University, Stanford, California 94305, USA*
[3]*Department of Physics, Stanford University, Stanford, California 94305, USA*
[4]*Department of Applied Physics, Stanford University, Stanford, California 94305, USA*

ErTe$_3$ is a model system used to explore thermal transport in a layered charge density wave (CDW) material. We present thermal diffusivity, resistivity, and specific-heat data: There is a sharp decrease in thermal conductivity parallel and perpendicular to the primary CDW at the CDW transition temperature. Yet, the resistivity changes more gradually. Using the Wiedemann-Franz law well above and below T_c a consistent description of the thermal transport applies with essentially independent electron and phonon contributions. In the critical regime, no such description is possible; the observed behavior corresponds to a strongly coupled electron-phonon critical "soup."

Unlike the standard paradigm [1,2], in more than one spatial dimension due to imperfect nesting, charge density wave (CDW) order (unlike superconducting order) only emerges for interactions greater than a critical strength. Generically, the "mechanism" involves strong electron-electron and electron-phonon interactions. Strong coupling is particularly reflected in large ratios of the induced gap to T_c. For the material in this Letter ErTe$_3$, the gap associated with the primary CDW transition at $T_{\mathrm{CDW1}} \approx 265$ K is $\Delta_1 \approx 175$ meV, implying $2\Delta_1/k_B T_{\mathrm{CDW1}} \approx 15$ [3,4]. Since weakly interacting quasiparticles and well-defined phonons give a good account of the physics at $T > T_{\mathrm{CDW1}}$ and at low temperatures deep in the ordered phase, it is conventional (following classical critical phenomena in metals) to adopt a phenomenological approach where low-energy quasiparticles and the bulk of phonons are weakly coupled to "critical modes" associated directly with the CDW transition. Our results challenge this standard perspective.

Electrical and thermal transport measurements provide important information about electronic structure and scattering processes in complex quantum materials. When transport is dominated by weakly interacting (emergent) elementary excitations, thermal conductivity can be expressed as the sum of electronic and phononic contributions, $\kappa \approx \kappa_{el} + \kappa_{\mathrm{ph}}$. Furthermore, for quasielastic scattering processes κ_{el} is related to electrical conductivity by the Wiedemann-Franz (WF) law, i.e., $\kappa_{el}/\sigma = L_0 T$, where $L_0 = \pi^2 k_B^2/3e^2 \approx 2.44 \times 10^{-8}$ W Ω K^{-2} is a universal constant. Observing this ratio indicates "standard" transport in a given electronic system, whereas significant violations of the WF law may indicate a breakdown of the quasiparticle description.

In this Letter, we examine electrical and thermal transports in the layered material ErTe$_3$, which exhibits CDW transitions at $T_{\mathrm{CDW1}} \approx 265$ and $T_{CDW2} \approx 160$ K. Here T_{CDW1} marks the onset of a "primary" CDW order with c-direction ordering vector q_{CDW1}. Below T_{CDW2} a "secondary" orthogonal a-direction CDW component q_{CDW2} appears (a and c are in-plane lattice parameters). Despite the nearly tetragonal crystal lattice ($a \sim c$ with b perpendicular), the phase at $T_{\mathrm{CDW1}} > T > T_{CDW2}$ has unidirectional CDW order, whereas the low-temperature CDW is bidirectional with inequivalent amplitudes in the directions. ErTe$_3$ is an ideal "model system" because it is stoichiometric and can be synthesized with a high degree of crystalline perfection and little disorder (very low residual resistivity—$\rho(T) < 1$ $\mu\Omega$ cm at low T and resolution-limited Bragg peaks associated with the CDW order). It boasts broad metallic bands with plasma frequency between 2.5 eV [3] and 5.8 eV [5] in the CDW state. Moreover, disorder can be explored systematically by Pd intercalation [6–8].

Our primary result is that thermal transport in a critical regime below T_{CDW1} appears inconsistent with quasiparticle transport. Assuming κ_{el} that satisfies the WF law, separate from κ_{ph}, one is forced to infer an unphysically large depression in lattice thermal transport. This demonstrative evidence for breakdown of the WF law and quasiparticle concept is strongly asymmetric, extending farther below T_{CDW1} than above it. In addition, we also observe: (i) Similar to other strongly interacting CDW systems, large anomalies are observed in the temperature derivative of the resistivity and reflectivity [Fig. 2(b)], which, assuming that Fisher-Langer theory [9] applies, stands in sharp contrast to the small heat-capacity anomaly [10]. The behavior of various linear-response tensors near criticality [Figs. 1(b) and 2(a)] depends strongly on direction. As T decreases, the a-direction resistivity ρ^a has a pronounced critical singularity at T_{CDW1} followed
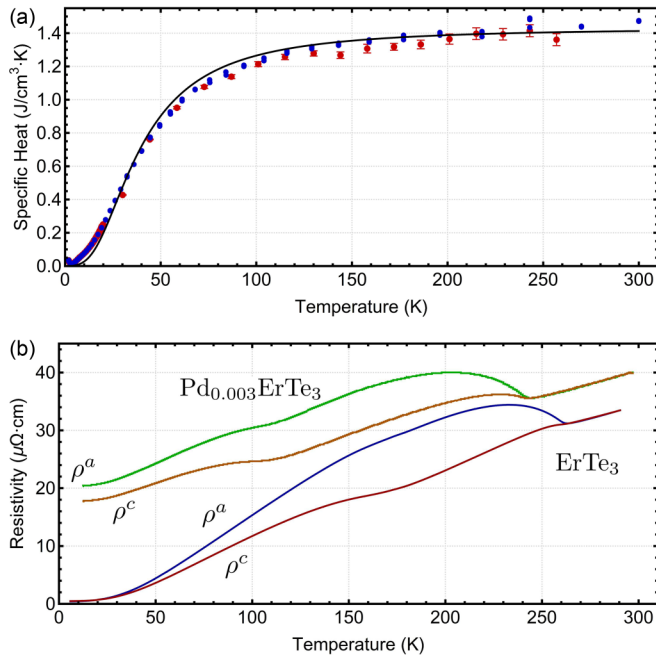
FIG. 1. (a) Specific heat of two ErTe₃ crystals. The solid line is a Debye model fit ($\theta_D = 160$ K). CDW transitions at $T_{\mathrm{CDW1}} \approx 265$ and $T_{CDW2} \approx 160$ K produce no prominent critical signatures. (b) Resistivity of similar crystals (blue: *a* axis and red: *c* axis) and of 0.3% Pd-intercalated crystal (green: *a* axis and orange: *c* axis). Note the decrease in the CDW transitions and increased residual resistivity for the intercalated sample.

by a broad maximum and subsequent low-temperature drop as previously discussed [11]. Conversely, the critical anomaly in ρ^c at T_{CDW1} is much weaker, and neither component shows any clear nonanalyticity at T_{CDW2}. In contrast, the thermal diffusivity has a large sharp decrease at T_{CDW1} along both the *a* and *c* directions, followed by a faster recovery along the *c* direction. Also evident from Fig. 2(a), the thermal diffusivity more closely resembles the temperature derivative of the resistivity. (iii) Thermal diffusivity in both directions increases markedly below T_{CDW2}, which through suppression of this effect by weak Pd intercalation are argued to be electronic in origin (Fig. 3).

ErTe₃ samples were grown using a Te self-flux technique, ensuring melt purity, and producing large crystals with a high degree of structural order [12]. Being air sensitive, ErTe₃ must be stored in an oxygen and moisture-free environment. Crystal orientation was determined with x-ray diffraction (XRD). Thermal diffusivity and differential reflectivity (dR/dT) were measured using a photothermal microscope [13]. Details of specific heat, resistivity, and thermal diffusivity measurements are described in the Supplemental Material (SM) [14]. Figure 1(a) shows specific heat of two ErTe₃ crystals over a wide temperature range. The data closely follow the Debye approximation with $\theta_D \approx 160$ K, including above and below both CDW transitions saturating at the high-temperature Dulong-Petit value. Previous measurements of the specific-heat anomaly at T_{CDW1} [10] find $\Delta c_p \approx 0.0144$ J/cm³ K, below the resolution of the present measurements, and surprisingly of "normal magnitude" given the large value of
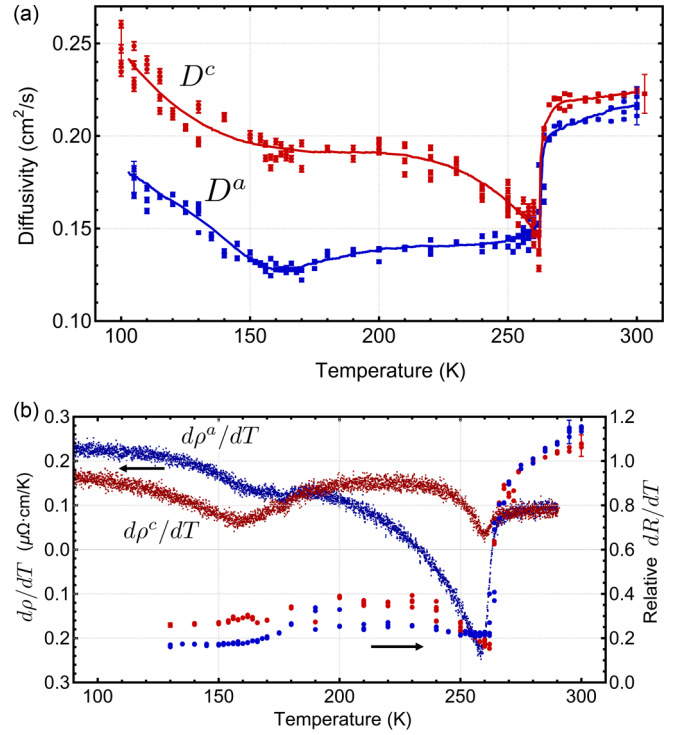

FIG. 2. (a) ErTe₃ thermal diffusivity measured using photothermal microscope showing CDW transitions at $T_{\mathrm{CDW1}} \approx 265$ and $T_{CDW2} \approx 160$ K. Scatter of data primarily associated with one-pixel control of measurement position and relative distance between heating and probing laser spots. Selected data near 100 and 300 K show representative 5% systematic uncertainty, see the SM [14]. Solid lines are guides to the eye. (b) Amplitude of temperature derivative of reflectivity—dR/dT normalized by this amplitude at $T_0 = 280$ K (full circles, right axis) vs temperature. Temperature derivative of the resistivity $d\rho/dT$, extracted from Fig. 1(b) (left axis) is shown for comparison. Blue: *a* axis and red: *c* axis. Selected data near 130 and 300 K show representative 5% systematic uncertainty.

$2\Delta_1/k_B T_{\mathrm{CDW1}} \approx 15$ inferred from angle-resolved photoemission spectroscopy measurements [4]. By contrast, both CDW transitions produce large anomalies in the thermal diffusivity data on a same-batch crystal as shown in Fig. 2(a).
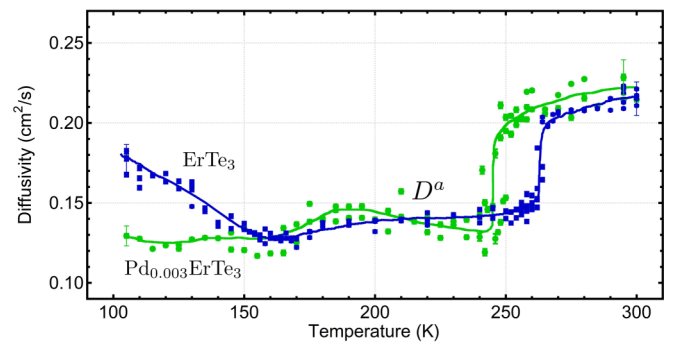

FIG. 3. Thermal diffusivity along the *a* axis of ErTe₃ (blue) and Pd₀.₀₀₃ErTe₃ (green). Selected data near 100 and 300 K show representative 5% systematic uncertainty, see the SM [14]. Solid lines to guide the eye.

Particularly, at T_{CDW1} diffusivity along both axes drops over a third from ~ 0.21 to ~ 0.14 cm^2/s.

Figure 1(b) shows resistivity data on same-batch crystals (see the SM [14] for determination of geometrical factors [16]). The trend in the data is similar to previously measured RTe$_3$ crystals [17], particularly, ErTe$_3$ [6,16], featuring a strong anomaly along the a axis (perpendicular to the primary CDW direction) at T_{CDW1} and only a weak wiggle along the c axis near T_{CDW2}. In contrast, thermal diffusivity along both axes sharply decreases at T_{CDW1} and gradually increases below T_{CDW2} [Fig. 2(a)]. However, these thermal diffusivity anomalies resemble more the features of the derivative of the resistivity $d\rho/dT$ as seen in Fig. 2(b). Similarly, the magnitude (see the SM [14]) of the temperature derivative of the reflectivity dR/dT at $h\nu \approx 1.5$ eV (820-nm wavelength) shows a large sharp decrease at T_{CDW1}, although here no anomaly is visible at T_{CDW2}.

Figure 3 demonstrates the effect of purposefully introduced weak disorder on the temperature dependence of thermal diffusivity. Focusing on the a axis (no noticeable effects appear in the c direction for this weak disorder [7]), we compare the diffusivity of Pd$_{0.003}$ErTe$_3$ to pure ErTe$_3$ [Fig. 2(a)]. Although T_{CDW1} is suppressed to 250 K, the sharp drop in diffusivity is not affected. However, below T_{CDW2} (here ~ 130 K) there is a striking intercalation induced difference; the pronounced upturn of the diffusivity in the pure material vanishes.

ErTe$_3$ resistivity was measured before [16,17] and the temperature dependence understood in terms of the material band structure [11]. Specifically, when the primary CDW forms along the c axis, the resistivity start increasing along the perpendicular a direction. Likewise, when the secondary CDW forms along the a axis, there is a larger change in $d\rho/dT$ along the c direction.

In a photothermal measurement, we extract thermal transport information by analyzing the phase delay in the change in reflectivity from a probed point on the sample surface due to a propagating heat wave originating from a pointlike source modulated at frequency ω. The reflected light amplitude $R(\nu)$, (where $\nu = c/\lambda$ is the probing light frequency with wavelength λ) detected at the probing point is proportional to dR/dT. Although within the heating spot the temperature may rise a few degrees, taking the system out of equilibrium, this small amount of heat quickly dissipates out not affecting the global temperature, whereas far from the heating spot guarantees very small δT and, thus, linear response (see Refs. [18,19] and the SM [14]). Optical reflectivity was previously measured on ErTe$_3$ [3,5] over the entire frequency range, exceeding the room-temperature plasma frequency, which depending on the global fit, is estimated between 20 000 cm^{-1} (500 nm) [3] to 47 000 cm^{-1} (213 nm) [5]. At our 820-nm probing wavelength, a Drude scattering rate ($1/\tau$) ~ 20 times smaller with a full Drude-Lorentz expression are needed to fit the experimental data in the whole frequency range [3,5]. Since the range of interband transition described by a set of Lorentz harmonic oscillators is temperature independent, it is reasonable to assume much of the temperature-dependent component of the reduction in reflectivity comes from the temperature dependence of the relaxation time, which is strongly affected by scattering from CDW fluctuations [3]. We then assume $R(\nu) = R_0(\nu) +$
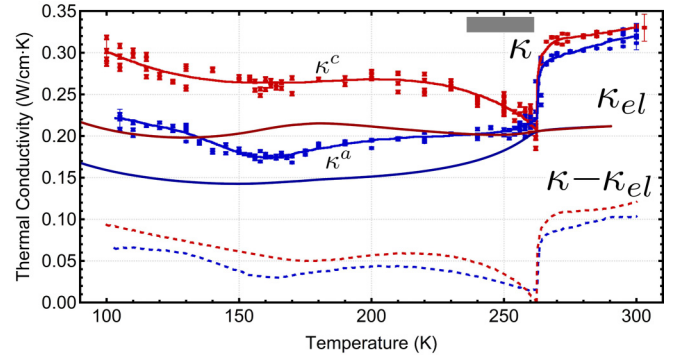

FIG. 4. Total thermal conductivity κ (solid line through the data is guide to eye), electronic component κ_{el} computed from ρ assuming WF law (solid), and $\Delta\kappa = \kappa - \kappa_{el}$, (dashed) as a function of T. Selected data near 100 and 300 K show representative 5% systematic uncertainty, see the SM [14]. The gray bar indicates critical region where the WF law breaks down.

$\Delta R(\nu\tau)$ (e.g., by extending the Hagen-Rubens relation to near-IR corresponding to our probing light $R(\nu) \simeq 1 - 2\sqrt{\nu\rho}$ with ρ as the Drude resistivity); thus, $dR/dT \propto d\tau/dT$.

In a seminal work, Fisher and Langer [9] showed that the leading (perturbative) effect of scattering of conduction electrons by classical (i.e., approximately static) critical modes leads to $d\rho/dT \propto c_{CDW}$, where c_{CDW} is the specific heat associated with critical fluctuations near a finite-T phase transition. Examining the temperature derivative of the resistivity, particularly the a direction, indeed, reveals what appears to be a broadened discontinuity at T_{CDW1}, similar to the behavior of the reflectivity. This mean-field-like form agrees with the shape of the anomaly observed in direct measurements of specific heat [10,20], although the relative strength of the anomaly is much weaker in those measurements [essentially invisible in Fig. 1(a)]. Despite similar behaviors at T_{CDW1}, at lower temperatures, $d\rho/dT$ and dR/dT exhibit substantially different thermal evolutions. The former, but not the latter, recovers rapidly to values comparable to the CDW transition [21]. Furthermore, near T_{CDW2}, $d\rho/dT$ shows a relatively weak but still clear critical anomaly, whereas the effect of the second CDW transition is difficult to discern in dR/dT.

More insight between electrical and thermal transports is obtained using their respective Einstein relations,

$$\sigma = \chi_{el}D_{el}; \quad \kappa = c_p D_Q, \tag{1}$$

with χ_{el} as the electronic compressibility, c_p as the total specific heat, D_{el} and D_Q as the electronic and heat diffusivities, respectively. Although χ_{el} is a response function of only the electron system, the specific heat of the material, particularly at high temperatures, may be lattice dominated. A simple kinetic approach where electrons and phonons transport heat in parallel channels implies $\kappa = \kappa_{el} + \kappa_{ph} = c_{el}D_{el} + c_{ph}D_{ph}$, where c_{el} and c_{ph} are the electronic and lattice specific heats and D_{el} and D_{ph} are the respective diffusivities.

The total thermal conductivity along the a and c axes can be calculated following Eq. (1) and using the measured specific heat and thermal diffusivity as is shown in Fig. 4 together with a best-fit guide to the eye curve. Assuming that WF law holds, we calculate the electronic thermal conductivity from the

resistivity $\kappa_{el} = L_0 T / \rho(T)$, also shown in Fig. 4. This allows us to define a "nonelectronic" contribution $\Delta\kappa \equiv \kappa - \kappa_{el}$. Although it is conventional to identify $\Delta\kappa$ with an independent phonon contribution $\Delta\kappa \leftrightarrow \kappa_{ph}$, it is apparent (discussed below) this is not plausible over much of the temperature range and especially in a region immediately below T_{CDW1} (gray bar in Fig. 4).

We first consider room-temperature thermal conductivity, above the CDW transitions. The value of the total thermal conductivity is very high compared to other chalcogenide-based CDW materials: $\kappa = 0.06$ W/cm K for TaSe$_3$ [22], 0.07 W/cm K for NbSe$_3$ [23], 0.05 W/cm K for (TaSe$_4$)$_2$I [24], 0.1 W/cm $\cdot$ K for 2H-TaSe$_2$ [25], 0.035 W/cm K for HfTe$_5$ [26], or 0.08 W/cm K at 370 K for 1T-TaS$_2$ [25]. By contrast, ErTe$_3$ exhibits $\sim$0.33 W/cm K at room temperature, more than three and up to ten times larger thermal conductivity than those compounds. However, using WF law and our measured resistivity to evaluate the electronic thermal conductivity, we obtain a value of $\Delta\kappa$ comparable in magnitude to these materials. Considering the much larger resistivities of these other materials, WF analysis yields a relative κ_{el}/κ of around 20% to 25% for most compounds, reaching 45% for NbSe$_3$ nanowires [23]. In all cases κ is very weakly T dependent in this range of temperature. One naturally identifies $\Delta\kappa \approx \kappa_{ph}$ as an essentially independent phonon contribution to the thermal conductivity—as commonly assumed.

WF law is expected to work at temperatures comparable and above the Debye temperature (θ_D), relying on quasielastic electron-phonon scattering applicable for modes whose characteristic frequencies, $\omega \ll k_B T / \hbar$ and all nearly critical modes due to critical slowing down. Thus, analysis of the CDW transition region, particularly, the anomaly at T_{CDW1}, which is $\sim$100 K above θ_D, implies a catastrophic breakdown of the WF approach. Although based on WF law, one would expect the critical anomaly in the total thermal conductivity to be weak similar to the resistivity, it is, in fact, pronounced and resembles the behavior of $d\rho/dT$. (Note the relatively weak specific heat anomaly at T_{CDW1}, primarily because the high transition temperature where the specific heat is already in the Dulong-Petit regime). More dramatically, if we use the WF law to subtract an electronic contribution to κ in the critical regime, we would be forced to conclude that the lattice contribution $\Delta\kappa$ mysteriously vanishes, at least, within $\sim$30° below T_{CDW1}—indicated by the gray bar in Fig. 4. This sharp decrease in $\Delta\kappa$ in ErTe$_3$ and the strong violation of the WF law is quite different from other one-dimensional CDW materials including Lu$_5$Ir$_4$Si$_{10}$ [27], LaAgSb$_2$ [28], and CuTe [29] where the WF is followed through T_{CDW} irrespective whether the electrical resistivity changes gradually or sharply. We know of no plausible physical mechanism that could produce such an effect. However, if inelastic scattering of the electrons from the critical modes plays a role in the breakdown of the WF law, this would be highly anomalous and suggests an unexpectedly intimate connection between the electronic and lattice degrees of freedom.

Below $\sim$240 K, $\Delta\kappa$ reaches $\sim$0.05 W/cm K, common to this type of materials, and, thus, again can be loosely interpreted as parallel lattice contribution. Using simple kinetic theory, our measured specific heat and typical longitudinal sound velocity of $\sim 2.8 \times 10^5$ cm/s [10,20], we obtain a mean

free path of $\sim$35 Å at $T = T_{CDW2}$, reduced from $\sim$80 Å above T_{CDW1}. Although below the primary CDW transition the phonon mean free path might be expected to increase reflecting reduced phonon-electron scattering, CDW fluctuations in the transition region and CDW formation below that temperature could be additional sources of phonon scattering. (By contrast, in other chalcogenide-based CDW materials κ is nearly constant with a slight tendency to increase with decreasing T over the same temperature range.) Over the same temperature range, the total and electronic thermal conductivities reach an anisotropic value of $\kappa^c/\kappa^a \approx \kappa_{el}^c/\kappa_e^a \approx 1.3$, reflecting the effect of the primary CDW transition at T_{CDW1}. Interestingly, this anisotropy is only weakly reduced below the secondary CDW transition at T_{CDW2} where the primary effect is an increase in all components of thermal transport. Although the increase in the putative lattice part below T_{CDW2} could be from further gapping of electronic states that decrease the phonon-electron scattering rate, the electronic increase in thermal conductivity simply reflects the increase in the mean free path of the remaining itinerant electrons. We check this hypothesis by introducing additional electron disorder scattering with a small concentration of intercalated Pd atoms ($\lesssim$1%), which does not markedly change the carrier density [6]. See the SM for similar response in $\Delta\kappa$ when there is $\sim$0.3% Pd intercalation of the material Pd$_{0.003}$ErTe$_3$ [14].

Figure 3 shows the effect of $\sim$0.3% Pd intercalation on the thermal diffusivity. Note the decrease in the primary CDW transition that follows the phase diagram in Ref. [6]. Focusing on a-axis transport where disorder shows a strong effect on the electronic structure [7], thermal diffusivity in Fig. 3 did not change much below T_{CDW1}, but the characteristic increase below T_{CDW2} is missing, consistent with the increased scattering observed in resistivity [Fig. 1(b)]. Although this points to an electronic effect, incomplete gapping of electronic states may also affect phonon-electron scattering [7,8].

Often, transport properties of metals are successfully understood based on the response of weakly interacting elementary excitations—fermionic quasiparticles and bosonic phonons. In past decades, various transport regimes in certain "highly correlated" materials have been identified where the validity of this approach has been questioned. However, it remains highly controversial to what extent conventional quasiparticle ideas can be extended without fundamental changes in approach to strongly interacting regimes where the quasiparticle identity is "marginally" maintained, or if entirely new paradigms (e.g., some form of "non-Fermi liquid" or novel fractionalized quasiparticles) are needed.

One approach to attack this problem has been to investigate the breakdown of quasiparticle picture near a quantum critical point. However, even at classical (finite-T) critical points, the existence of nontrivial critical exponents describing behavior in the critical regime provides clear evidence that critical modes themselves cannot have a quasiparticle description. None-the-less, often, where, e.g., Fisher-Langer theory gives good account of transport anomalies, a treatment involving well-defined conduction electrons (and, presumably, phonons) weakly scattered by critical modes implies that the conventional mechanism of transport theory applies even in the critical regime.

The dramatic failure of this approach to adequately describe thermal transport in ErTe$_3$, most dramatically in the $\sim$30 K range below T_{CDW1}, may potentially indicate a simpler context to study the quasiparticle paradigm breakdown. The discrepancies in the critical dependences of thermal conductivity and resistivity in this regime imply a complete breakdown of the WF law, the existence of independent electronic quasiparticles and phonon modes or both. Indeed, the observed behavior may more adequately be described as a strongly coupled electron-phonon critical "soup."

CDW formation is a common phenomenon in quasi-low-dimensional materials, arising from a variety of mechanisms. Although thermal transport measurements have not been widely performed for such materials, they exist for many well-known canonical examples, and in no cases has such dramatic violation of the WF law been deduced. This raises associated questions as why the effect should be so pronounced in this particular material system given the ubiquity of CDW compounds (for a recent survey of CDW systems, see, e.g., Ref. [30]). A wider survey of related materials might reveal that this effect is not unique to the rare-earth tritellurides,

yet for now ErTe$_3$ occupies a unique position among known CDW compounds and presents an entirely new opportunity to explore unconventional transport properties of strongly interacting metals.

---

[1] R. E. Peierls, *Quantum Theory of Solids* (Clarendon, Oxford, 1955).

[2] H. Fröhlich, On the theory of superconductivity: The one-dimensional case, Proc. R. Soc. A **223**, 296 (1954).

[3] F. Pfuner, P. Lerch, J.-H. Chu, H.-H. Kuo, I. R. Fisher, and L. Degiorgi, Temperature dependence of the excitation spectrum in the charge-density-wave ErTe$_3$ and HoTe$_3$ systems, Phys. Rev. B **81**, 195110 (2010).

[4] R. G. Moore, V. Brouet, R. He, D. H. Lu, N. Ru, J.-H. Chu, I. R. Fisher, and Z.-X. Shen, Fermi surface evolution across multiple charge density wave transitions in ErTe$_3$, Phys. Rev. B **81**, 073102 (2010).

[5] B. F. Hu, B. Cheng, R. H. Yuan, T. Dong, A. F. Fang, W. T. Guo, Z. G. Chen, P. Zheng, Y. G. Shi, and N. L. Wang, Optical study of the multiple charge-density-wave transitions in ErTe$_3$, Phys. Rev. B **84**, 155132 (2011).

[6] J. A. W. Straquadine, F. Weber, S. Rosenkranz, A. H. Said, and I. R. Fisher, Suppression of charge density wave order by disorder in Pd-intercalated ErTe$_3$, Phys. Rev. B **99**, 235138 (2019).

[7] A. Fang, J. A. W. Straquadine, I. R. Fisher, S. A. Kivelson, and A. Kapitulnik, Disorder-induced suppression of charge density wave order: Stm study of pd-intercalated ErTe$_3$, Phys. Rev. B **100**, 235446 (2019).

[8] A. Fang, A. G. Singh, J. A. W. Straquadine, I. R. Fisher, S. A. Kivelson, and A. Kapitulnik, Robust superconductivity intertwined with charge density wave and disorder in pd-intercalated ErTe$_3$, Phys. Rev. Research **2**, 043221 (2020).

[9] M. E. Fisher and J. S. Langer, Resistive Anomalies at Magnetic Critical Points, Phys. Rev. Lett. **20**, 665 (1968).

[10] M. Saint-Paul, G. Remenyi, C. Guttin, P. Lejay, and P. Monceau, Thermodynamic and critical properties of the charge density wave system ErTe$_3$, Physica B **504**, 39 (2017).

[11] A. A. Sinchenko, P. D. Grigoriev, P. Lejay, and P. Monceau, Spontaneous Breaking of Isotropy Observed in the Electronic Transport of Rare-Earth Tritellurides, Phys. Rev. Lett. **112**, 036601 (2014).

[12] N. Ru and I. R. Fisher, Thermodynamic and transport properties of YTe$_3$, LaTe$_3$, and CeTe$_3$, Phys. Rev. B **73**, 033101 (2006).

[13] J. Zhang, E. M. Levenson-Falk, B. J. Ramshaw, D. A. Bonn, R. Liang, W. N. Hardy, S. A. Hartnoll, and A. Kapitulnik, Anomalous thermal diffusivity in underdoped YBa$_2$Cu$_3$O$_{6+x}$, Proc. Natl. Acad. Sci. USA **114**, 5378 (2017).

[14] See Supplemental Material at http://link.aps.org/supplemental/10.1103/PhysRevB.104.L241109 for details of specific heat, resistivity, and thermal diffusivity measurements which includes Ref. [15].

[15] S. Mumford, T. Paul, E. Kountz, and A. Kapitulnik, Journal of Applied Physics **128**, 175105 (2020).

[16] P. Walmsley and I. R. Fisher, Determination of the resistivity anisotropy of orthorhombic materials via transverse resistivity measurements, Rev. Sci. Instrum. **88**, 043901 (2017).

[17] N. Ru, C. L. Condron, G. Y. Margulis, K. Y. Shin, J. Laverock, S. B. Dugdale, M. F. Toney, and I. R. Fisher, Effect of chemical pressure on the charge density wave transition in rare-earth tritellurides RTe$_3$, Phys. Rev. B **77**, 035114 (2008).

[18] J. T. Fanton, D. B. Mitzi, A. Kapitulnik, B. T. Khuri-Yakub, G. S. Kino, D. Gazit, and R. S. Feigelson, Photothermal measurements of high tc superconductors, Appl. Phys. Lett. **55**, 598 (1989).

[19] Z. Hua, H. Ban, and D. H. Hurley, The study of frequency-scan photothermal reflectance technique for thermal diffusivity measurement, Rev. Sci. Instrum. **86**, 054901 (2015).

[20] M. Saint-Paul and P. Monceau, Phenomenological approach of the thermodynamic properties of the charge density wave systems, Philos. Mag. **101**, 598 (2021).

[21] N. Lazarević, Z. V. Popović, R. Hu, and C. Petrovic, Evidence of coupling between phonons and charge-density waves in ErTe$_3$, Phys. Rev. B **83**, 024302 (2011).

[22] B. Zawilski, R. Littleton IV, N. Lowhorn, and T. Tritt, Observation of a two level thermal conductivity in the low-dimensional materials, Solid State Commun. **150**, 1299 (2010).

[23] L. Yang, Y. Tao, J. Liu, C. Liu, Q. Zhang, M. Akter, Y. Zhao, T. T. Xu, Y. Xu, Z. Mao, Y. Chen, and D. Li, Distinct signatures of electron-phonon coupling observed in the lattice thermal conductivity of NbSe$_3$ nanowires, Nano Lett. **19**, 415 (2019).

[24] R. S. Kwok and S. E. Brown, Thermal Conductivity of the Charge-Density-Wave Systems K$_{0.3}$MoO$_3$ and (TaSe$_4$)$_2$I Near the Peierls Transition, Phys. Rev. Lett. **63**, 895 (1989).

[25] M. D. Núñez-Regueiro, J. M. Lopez-Castillo, and C. Ayache, Thermal Conductivity of $1T - TaS_2$ and $2H - TaSe_2$, Phys. Rev. Lett. **55**, 1931 (1985).

[26] B. M. Zawilski, R. T. Littleton, and T. M. Tritt, Description of the parallel thermal conductance technique for the measurement of the thermal conductivity of small diameter samples, Rev. Sci. Instrum. **72**, 1770 (2001).

[27] Y.-K. Kuo, C. S. Lue, F. H. Hsu, H. H. Li, and H. D. Yang, Thermal properties of lu$_5$ir$_4$si$_{10}$ near the charge-density-wave transition, Phys. Rev. B **64**, 125124 (2001).

[28] C. S. Lue, Y. F. Tao, K. M. Sivakumar, and Y. K. Kuo, Weak charge-density-wave transition in LaAgSb$_2$ investigated by transport, thermal, and NMR studies, J. Phys.: Condens. Matter **19**, 406230 (2007).

[29] C. N. Kuo, R. Y. Huang, Y. K. Kuo, and C. S. Lue, Transport and thermal behavior of the charge density wave phase transition in cute, Phys. Rev. B **102**, 155137 (2020).

[30] M. Saint-Paul and P. Monceau, Survey of the thermodynamic properties of the charge density wave systems, Adv. Condens. Matter Phys. **2019**, 2138264 (2019).